Cyclic Shear Behaviour of Clay Subjected to Initial Shear Stress

Masayuki HYODO*, Motohiro SUGIYAMA**, Noriyuki YASUFUKU*,
Hidekazu MURATA* and Yoriharu KAWATA**

(Received July 23, 1993)

Abstract

A series of undrained cyclic triaxial compression tests has been performed on a high plasticity marine clay. Testing was performed under various combinations of initial static and subsequent cyclic shear stress on isotropically and anisotropically consolidated specimens. Additionally, monotonic triaxial compression and extension tests were also performed on the same clay with the same initial condition. The cyclic shear strength is first considered, and then, the accumulated shear strain is investigated related to the effective stress ratio at the peak cyclic stress. Based on the experimental results, a semi-empirical model is proposed for evaluating the development of residual shear strain during cyclic loading. The model successfully explains the behaviour of clay subjected to various magnitudes of initial static and subsequent cyclic shear stresses.

Introduction

In considering earthquake design problems, interst has focused on the liquefaction of saturated sands. During earthquakes clays have been considered to be stable in comparison with sands. However, serious damage to structures sited on thick clay layers was reported in the 1985 Mexico Earthquake (Seed et al.[1], Mendoza et al.[2]). Large ground deformations due to the amplification of seismic motion is recognized as a characteristic of clay behaviour during earthquakes. Additionally, a lot of fill collapses as shown in Fig.1 were caused in Japan by the failure of clay base layers in 1964 Niigata Earthquake and 1978 Miyagiken-oki Earthquake (Sasaki et al.[3]).

Such case histories in the previous earthquakes bring up a question whether clays are really more stable than sands during the earthquakes. The comparison between the cyclic strengths for sand and clay has been done by the laboratory tests, such as cyclic triaxial tests on isotropically consolidated specimens which simulate the horizontally layers. In this condition, clay may behave more stablly than sand and pore pressure in clay may not develop up to the initial effective confining stress. However, practically most designs have been concerned about the base grounds below structures or elements in slopes whose soil elements are generally subjected to the initial static shear stresses. In order to simulate these situations, the cyclic triaxial tests on anisotropical-

*Department of Civil Engineering.
**Graduate Student, Department of Civil Engineering.

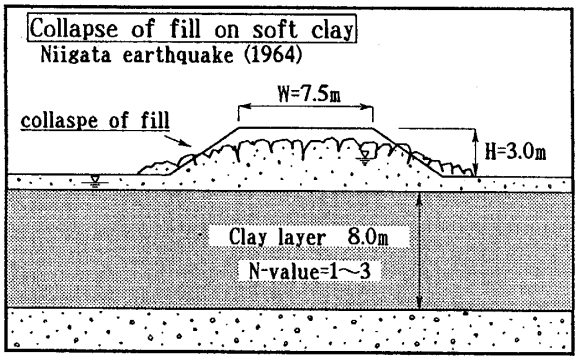

Fig.1 A case history of fill-collapse on soft clay in 1964 Niigata Earthquake[3]

ly consolidated specimens or cyclic simple shear tests subjected to initial static shear stresses are performed.

On the other hand, in the design of offshore platforms against wave loading, the cyclic properties of clays have been investigated and used in practical design methods for the stability of offshore platforms (Andersen et al.[4),5]). Although clay dynamics have not been investigated as widely as the liquefaction of sands, potentially a lot of dynamic probfems could arise in especially with the increasing construction of various structures founded on clay layers.

A series of undrained cyclic triaxial tests has been performed on a plastic marine clay in this study. Testing was carried out under various combinations of initial static and cyclic shear stresses which are those expected on soil elements subjected to cyclic loading in the vicinity of structures. Based on the experimental results, a semi-empirical model for predicting residual shear strain developed during cyclic loading is proposed which will be a useful tool for practical design methods.

Testing Procedure

Monotonic and cycfic triaxial compression tests were carried out on resedimented Itsukaichi clay, a marine clay sampled on the south coast of Hiroshima in Japan. Its index properties are $G_s=2.552$, $w_L=124.2\%$, $w_p=51.4\%$ and $I_p=72.8$. In order to prepare the resedimented sample, the clay slurry mixed with an initial water content of 260% was poured into a consolidation vessel and was then preconsolidated by a vertical pressure of 50kPa. Then the specimens with initial dimensions of 50mm in diameter and 100mm in height were trimmed from the clay block formed by the consolidation vessel. In order to get a high degree of saturation, a back pressure of 100kPa had been applied for 1 hour. B-values of more than 0.96 were observed in all specimens used in the tests. The specimens were initially consolidated isotropically and then consolidated anisotropically by applying a static deviator stress at a constant mean principal stress of 200kPa in the triaxial cell.

A sinusoidal cyclic axial load was applied at a frequency of 0.02Hz, which was decided after investigating the homogeneity of the water content distribution in the specimens under undrained cyclic loading (Yamamoto et al.[6], Hyodo et al.[9]). The

Table 1 Conditions of cyclic triaxial tests on clay

Test No.	p_c (kPa)	σ_{rc}' (kPa)	OCR	q_s (kPa)	q_{cyc} (kPa)	f (Hz)	w_i (%)	e_i	e_c
HN11	200	200	1	0	138.8	0.02	98.9	2.454	1.737
HN12	200	200	1	0	112.8	0.02	97.2	2.422	1.726
HN14	200	200	1	0	98.8	0.02	98.5	2.446	1.728
HN13	200	200	1	0	94.2	0.02	97.3	2.412	1.700
HS01	200	180	1	60	159.2	0.02	95.0	2.348	1.658
HS02	200	180	1	60	123.8	0.02	94.0	2.306	1.661
HS04	200	180	1	60	99.0	0.02	91.2	2.239	1.588
HS05	200	160	1	120	121.4	0.02	88.2	2.192	1.577
HS06	200	160	1	120	99.0	0.02	90.8	2.238	1.568
HS14	200	160	1	120	81.8	0.02	89.0	2.198	1.563
HS07	200	160	1	120	72.2	0.02	89.4	2.201	1.555
HS10	200	140	1	180	122.6	0.02	88.2	2.152	1.501
HS08	200	140	1	180	99.0	0.02	87.9	2.171	1.509
HS09	200	140	1	180	76.2	0.02	90.3	2.216	1.512
HS11	200	120	1	240	94.8	0.02	88.7	2.173	1.439
HS12	200	120	1	240	60.4	0.02	89.4	2.197	1.485
HS13	200	120	1	240	48.8	0.02	90.7	2.209	1.477

conditions for the cyclic triaxial tests are summarized in Table 1. Stress parameter p and q are used for representing effective mean principal stress, $p=(\sigma'_a+2\sigma'_r)/3$, and deviator stress, $q=\sigma_a-\sigma_r$, respectively. σ_{rc}' and p_c means the lateral pressure and the value of p after consolidation, respectively. Cyclic loading tests were performed over a range of initial static deviator stress q_s varying from 0 to 240kPa at 60kPa intervals for normally consolidated specimens. From four to six magnitudes of cyclic deviator stress q_{cyc} were combined with each static deviator stress level so that both reversal and non-reversal of cyclic shear stresses were simulated.

Strain controlled undrained monotonic triaxial compression and extension tests were also performed on samples with the same initial condition affer isotropic and anisotropic consolidation. They were executed by applying a monotonic axial load with a strain rate of 0.1%/min. These tests were performed in order to compare their behaviour with the results of cyclic triaxial tests. The conditions for the

Table 2 Conditions of monotonic triaxial tests on clay

Test No.	p_c (kPa)	σ_{rc}' (kPa)	OCR	q_s (kPa)	w_i (%)	e_i	e_c	Mode
HN03C	200	200	1	0	105.9	2.632	1.837	Compression
HN05E	200	200	1	0	103.1	2.568	1.819	Extension
HS01C	200	180	1	60	92.5	2.311	1.669	Compression
HS05E	200	180	1	60	89.3	2.216	1.650	Extensio
HS02C	200	160	1	120	89.2	2.207	1.613	Compression
HS06E	200	160	1	120	90.3	2.228	1.599	Extension
HS03C	200	140	1	180	88.0	2.161	1.566	Compression
HS07E	200	140	1	180	90.3	2.241	1.562	Extension
HS04C	200	120	1	240	89.6	2.210	1.529	Compression
HS09E	200	120	1	240	90.9	2.246	1.510	Extension

monotonic triaxial tests are shown in Table 2.

Cyclic Behaviour of Normally Consolidated Clay

The cyclic triaxial tests were performed using both reversal and non-reversal of cyclic shear stresses. Typical effective stress paths during cyclic loading for normally consolidated clay in each loading pattern are presented in Fig.2. The failure envelopes obtained from undrained monotonic tests are also drawn in each figure. The slopes of the envelopes for compression and extension are $M_c=1.560$ and $M_e=1.456$, respectively. In the isotropically consolidated case, as shown in Fig.2 (a), the effective stress path moved towards the failure envelopes during cyclic loading and finally it traced a steady loop which reached the failure envelopes on both compression and extension sides. Pore pressure measured at the bottom of the specimen through the pedestal did not develop up to the initial confining stress. On the other hand, in the anisotropically consolidated results, as shown in Fig.2 (b) and (c), the effective stress paths moved until their upper end touched the failure line on the compression side. Further, it was found that the stress paths crossed the failure envelopes at the final stage of cyclic loading. This phenomenon was also observed by Hyde and Ward [10] and was explained as the samples becoming more heavily overconsolidated under undrained conditions. Although there is some stress reversal from the compression to the extension side in the results presented in Fig.2 (b), the failure mode is almost the same as the non-reversal case shown in Fig.2 (c).

Typical results demonstrating the relationship between cyclic deviator stress and axial strain are presented in Fig.3. For comparison, the results of cyclic triaxial tests on both isotropically and anisotropically consolidated Toyoura sand with $Dr=70\%$

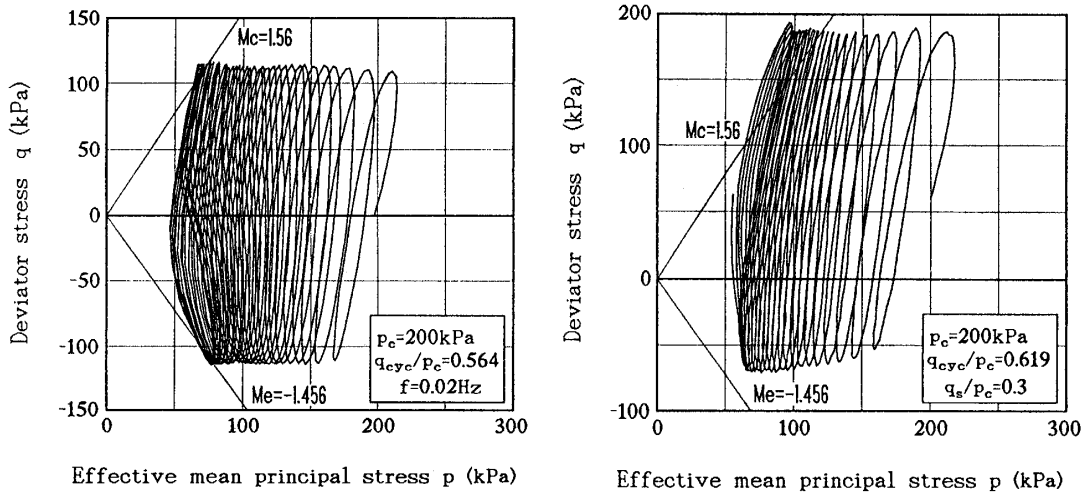

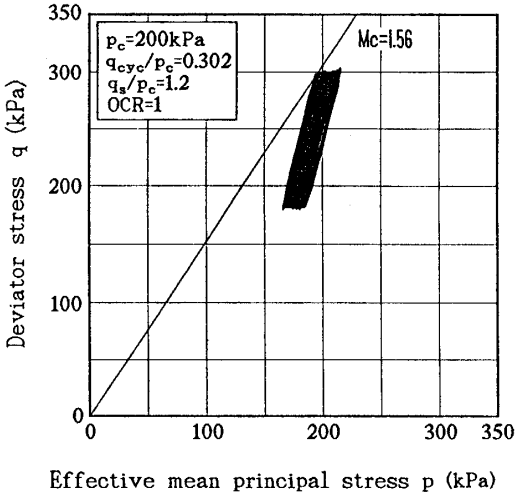

Fig.2 Effective stress paths in the cases of, (a): isotropically consolidated, (b): anisotropically consolidated with stress reversal, (c): anisotropically consolidated with non-reversal

(Hyodo et al.[7]) are presented in Figs.4 (a) and (b), respectively. A large amplitude of cyclic axial strain was observed at the failure stage in the isotropically consolidated clay as shown in Fig.3 (a). The behaviour looks similar to that of sand (Fig.4 (a)) when liquefaction is achieved. On the other hand, the residual strain was predominant for the anisotropically consolidated results shown in Figs.3 (b) and (c). The increment of strain in clay became larger with increasing number of cycles and specimens were brought to failure, while the sand behaved stablly and never reached failure in the non-reversal condition as shown in Fig.4 (b). Furthermore, it should be noted that an increase in the residual strain of clay during a cycle was triggered when the stress paths approached the critical state line. Therfore, clay is considered to be more unstable than sand in the non-reversal cyclic stress condition.

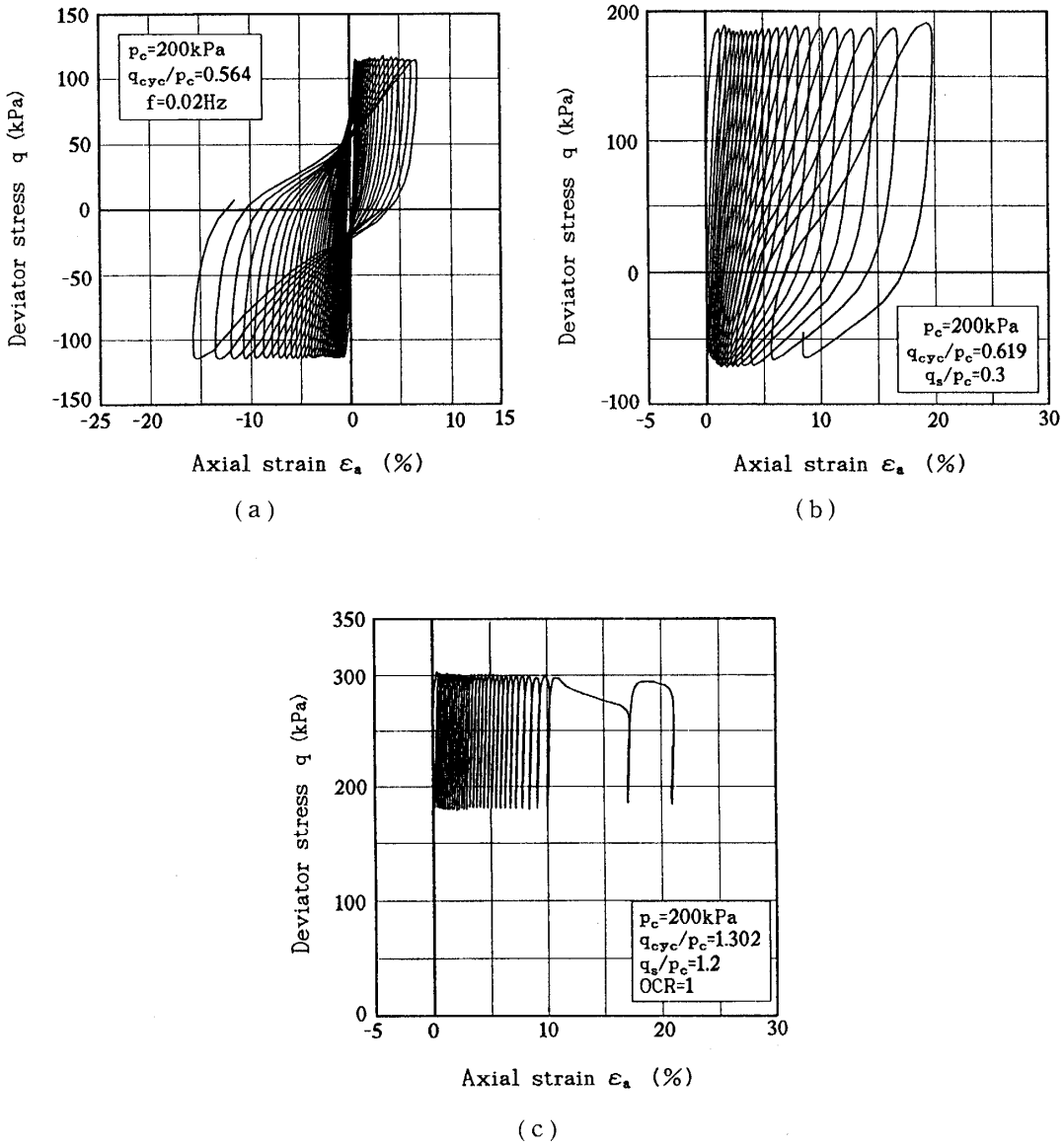

Fig.3 Relationships between deviator stress and axial strain for clay in the cases of, (a): isotropically consolidated, (b): anisotropically consolidated with stress reversal, (c): anisotropically consolidated with non-reversal

Undrained Monotonic Triaxial Behaviour

Undrained monotonic compression and extension tests were performed under the conditions as shown in Table 2. All test results are presented together in Figs.5 and 6 which illustrate the effective stress paths and the relationship between deviator stress and axial strain, respectively. While both compression and extension tests were carried out from several different anisotropically consolidated conditions with various initial deviator stresses, these initial deviator stresses were applied only on the compression side. Considering the effective stress path on the compression side, after reaching a local peak deviator stress, strain softening behaviour appeared. On the extension side, stress paths for anisotropically consolidated specimens trace almost the same path

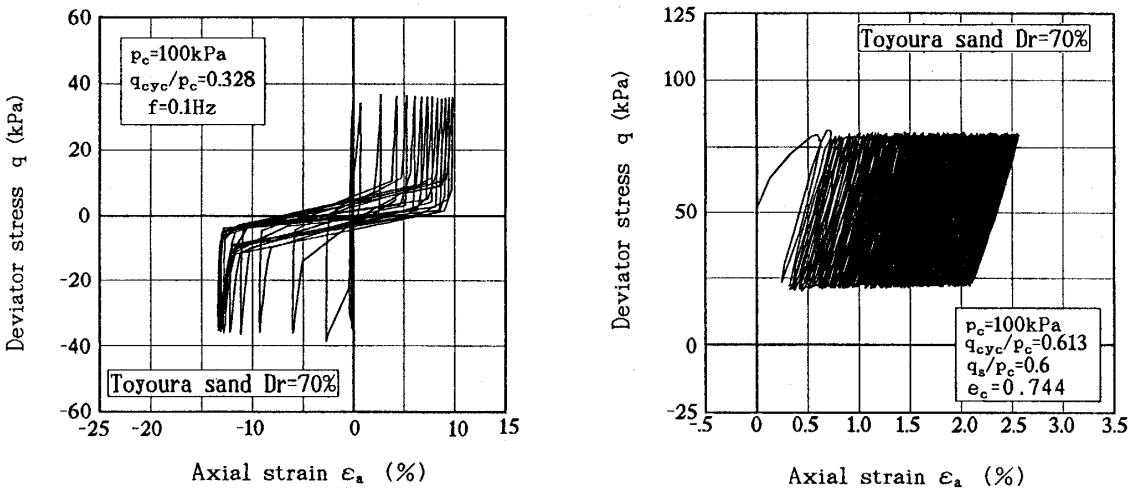

(a) (b)

Fig.4 Relationships between deviator stress and axial strain for sand in the cases of, (a): isotropically consolidated, (b): anisotropically consolidated condition

except the case for the highest initial static deviator stress ratio $q_s/p_c=1.2$ which showed a dilative manner at the final stage.

The stress-strain curve for compression tests show that the softening behaviour appears after reaching the peak strength at a fairly small strain stage. It is found that the larger the initial deviator stress, the larger the decrement of strength during softening. On the other hand extension tests exhibit only hardening behaviour.

Evaluation of Cumulative Axial Strain During Cyclic Loading

Attempts were made to quantify the cumulative peak axial strain corresponding to the peak cyclic stress on the compression side in each loading cycle. The cumulative peak axial strains ε_p from all tests were related using an effective stress ratio η_p ($=q_s/p$) which is the value of peak deviator stress divided by the mean effective principal stress of each peak cyclic stress. Fig.7 is the relationship between peak axial strain and effective stress ratio. It can be seen in the figure that there is a unique relationship between peak axial strain and effective stress ratio although the magnitudes of initial static and applied cyclic deviator stresses are different one another. Furthermore, it is found in these figures that although the starting points are different for each initial static deviator stress, the main part of the relations are approximated by a unique hyperbola given by the following equation.

$$\varepsilon_p = \eta_p/(a_1+b_1\eta_p) \tag{1}$$

where a_1 and b_1 are the experimental parameters and were determined as $a_1=2.0$, $b_1=-1.0$. The similar relation was also observed in anisotropically consolidated sand (Hyodo et al.[7]).

Cyclic Shear Strength

It is convenient to make a unified definition of cyclic shear strength in both reversal and non-reversal stress conditions. In the relationship in Fig.7, the cyclic failure is defined as the cummulative peak axial strain $\varepsilon_p = 10\%$ because the hyperbola shown in Fig.7 approaches the asymptotic at about $\varepsilon_p = 10\%$. Taking this failure criterion in both the reversal and non-reversal regions, the relationship between the cyclic deviator

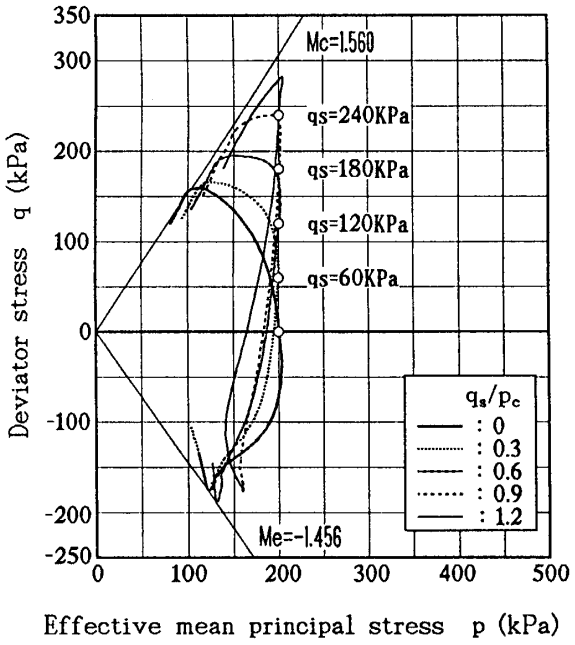

Fig.5 Effective stress paths in monotonic tests with various initial static deviator stress

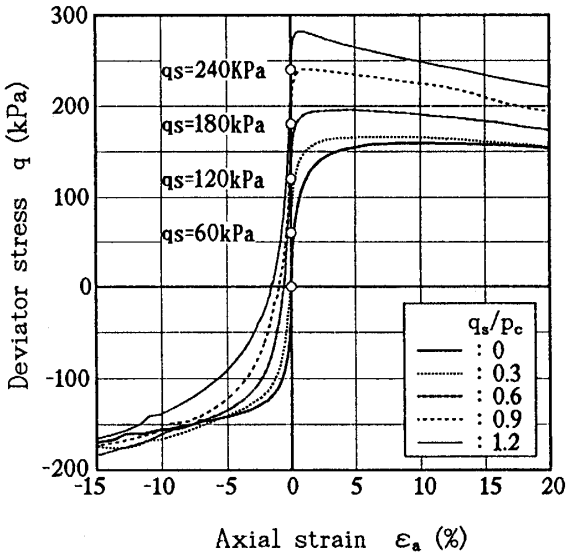

Fig.6 Relationship between deviator stress and axial strain in monotonic tests with various initial static deviator stress

stress ratio and the number of cycles required to cause failure for each initial static deviator stress q_s is represented as shown in Fig.8. The cyclic strength for the clay with zero initial static deviator stress ratio is determined by the 10% of double amplitude of axial strain, *DA* instead of ε_p. It is observed in the figure that the cyclic shear strength for clay decreases with increasing initial static deviator stress. In order to compare the oyclic shear strength for clay and sand, the cyclic shear strength curves for isotropically consolidated clay and Toyoura sand with $Dr=50\%$ and 70% (Hyodo et al.[7]) are represented in Fig.9. In isotropically consolidated condition, the cyclic strength for clay is about two or three times as high as that for sand.

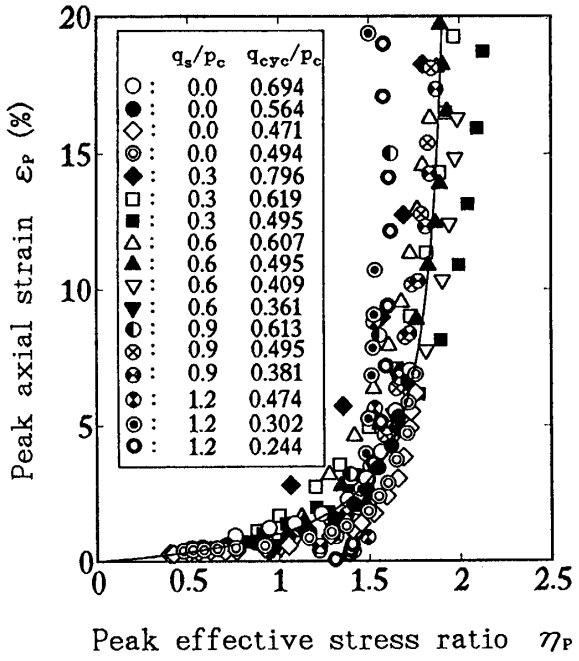

Fig.7 Relationship between accumulated peak axial strain and effective stress ratio during cyclic loading

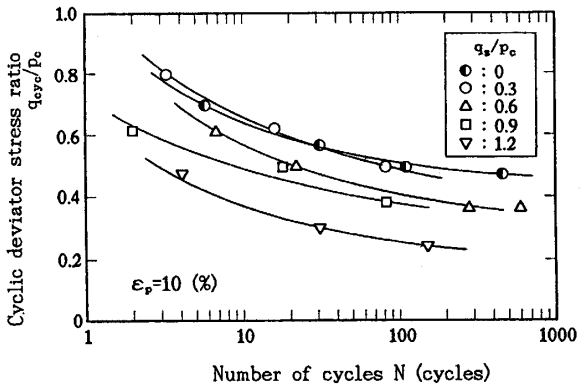

Fig.8 Relationship between cyclic deviator stress ratio q_{cyc}/p_c and number of cycles to cause peak axial strain $\varepsilon_p=10\%$

Then, the variations of cyclic deviator stress ratio required to cause $\varepsilon_p = 10\%$ in 20 cycles with initial static deviator stress ratio for both clay and sand are summarized in Fig.10. It is found in both figures that the cyclic deviator stress ratio to cause failure in clay decreases with increasing initial static deviator stress. On the other hand, cyclic shear strength for sand increases with increasing initial deviator stress. In isotropically consolidated condition, the cyclic strength for clay is certainly greater than that for sand. However, the inequality is reversed at a certain initial static deviator stress. Especially at the non-reversal region, cyclic shear strength for clay is far lower than that for sand. Therefore, it appeared that the clay subjected to initial static shear stress, such as a layer founded by the structure, is more unstable than sand during cyclic loading.

For the purpose of development of the empirical model, redefining the cyclic strength as $R_f = \{(q_{cyc}+q_s)/p_c\}_f$, it can be approximated by straight lines of a logarithmic form. These are parallel straight lines for each initial static deviator stress as shown in Fig.11 in which the cyclic strength for $q_s/p_c=0$ is also illustrated and formulated by Eq. (2). The variations of cyclic strengths with initial static deviator stress ratio for 5, 20 and 100 cycles with initial static deviator stress ratio are illustrated in Fig.12.

$$R_f = \{(q_{cyc}+q_s)/p_c\}_f = \kappa N^{\beta} \tag{2}$$

where $\beta = -0.088$ and $\kappa = 1.0 + 1.5 q_s/p_c$.

Relative Effective Stress Ratio and Cyclic Shear Strength Ratio

In the previous section, a unified cyclic shear strength, $R_f = \{(q_{cyc}+q_s)/p_c\}_f$, applicable to all the loading patterns was defined. In order to represent the undrained cyclic behaviour of clay, let us introduce the following two parameters. The first parameter is defined as an index of the possibility of cyclic failure, R/R_f which is the ratio of the peak cyclic deviator stress, $R = q_s + q_{cyc}$, to the cyclic shear strength, in a given number of cycles. R/R_f, named cyclic shear strength ratio, is equivalent to the reciprocal of the safety factor against cyclic failure. When the magnitude of R is constant, R/R_f increases with increasing number of cycles and varies from zero at non-loading to unity at failure.

The second parameter is defined as:

$$\eta^* = (\eta_p - \eta_s)/(\eta_f - \eta_s) \tag{3}$$

where η_p is the effective stress ratio at the peak of the cyclic stress in each cycle, η_s is the effective stress ratio for initially consolidated conditions and η_f is the effective stress ratio at failure. This parameter, η^*, therefore, indicates the relative effective stress ratio between the initial point and the final point in $p-q$ space as shown in Fig. 13. These parameters were originally introduced for sand by Hyodo et al.[7] and also applied to isotropically consolidated clay (Hyodo et al.[8]). By correlating the values

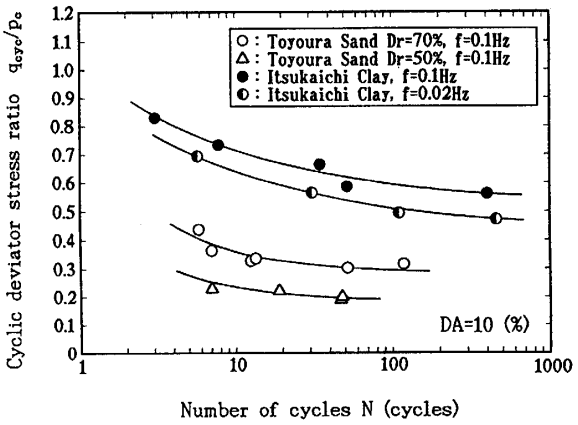

Fig.9 Relationship between cyclic deviator stress ratio q_{cyc}/p_c and number of cycles to cause $DA=10\%$ for isotropically consolidated sand and clay

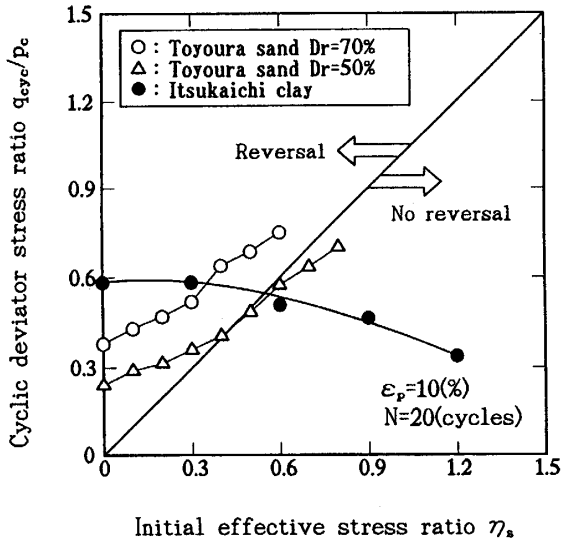

Fig.10 Relationship between normalized cyclic deviator stress and initial static deviator stress to cause $\varepsilon_p=10\%$ at 20 cycles for sand and clay

of both parameters, we obtain Fig.14 for each q_s/p_c. Despite the difference in initial static and subsequent cyclic deviator stresses, the best fit curve for each relation is given by a unique curve formulated by the following equation:

$$\eta^*=R/R_f/\ \{a_2-(a_2-1)R/R_f\} \tag{4}$$

where a_2 was determined experimentally as 6.5.

Cyclic-induced peak axial strain is calculated by the following process:

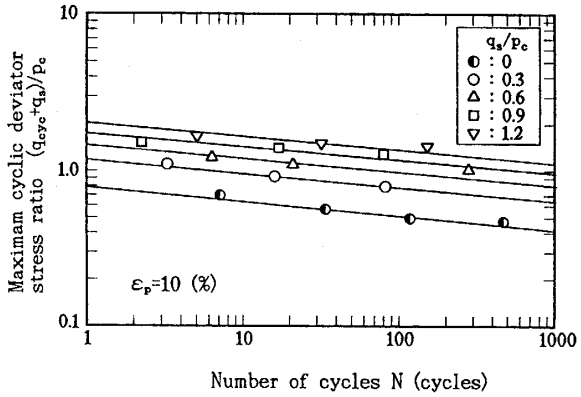

Fig.11 Relationship between cyclic deviator stress ratio $(q_s+q_{cyc})/p_c$ and number of cycles to cause peak axial strain $\varepsilon_p=10\%$ for clay

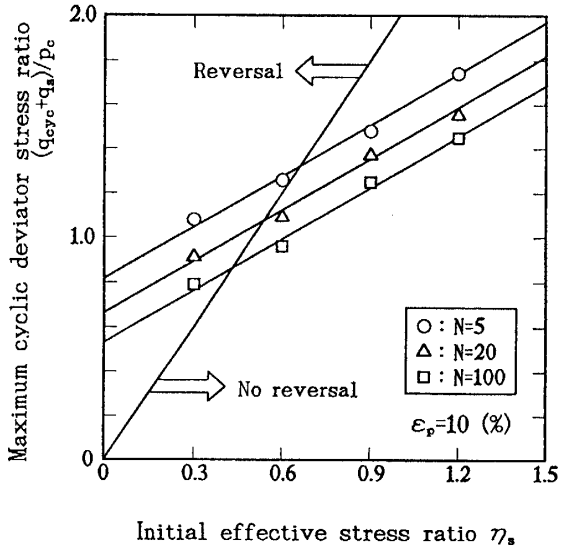

Fig.12 Relationships between cyclic strength R_f and initial static deviator stress ratio to cause $\varepsilon_p=10\%$ at 5, 20, 100 cycles

(1) The cyclic shear strength R_f for the desired initial static deviator stress and number of stress cycles is decided through the relationship given by Eq.(1). Then the cyclic shear strength ratio R/R_f is obtained by dividing the applied stress ratio R by the strength R_f.

(2) The relative effective stress ratio η^* is obtained by substituting R/R_f into the relationship between η^* and R/R_f given by Eq.(4).

(3) The effective stress ratio η_p at the peak cyclic stress of a given stress cycle is

calculated by the following rewritten form of Eq.(3).

$$\eta_p = \eta^*(\eta_f - \eta_s) + \eta_s \tag{5}$$

(4) The pore pressure at the peak axial strain is calculated substituting η_p into the following equation.

$$u_p = p_c + q_{cyc}/3 - (q_s + q_{cyc})/\eta_p \tag{6}$$

(5) The peak axiaf strain is evaluated by substituting η_p into Eq.(1).

If these steps are repeated from the first to the last stress cycle, the cumulative peak pore pressures and peak axial strains can be predicted against number of cycles during

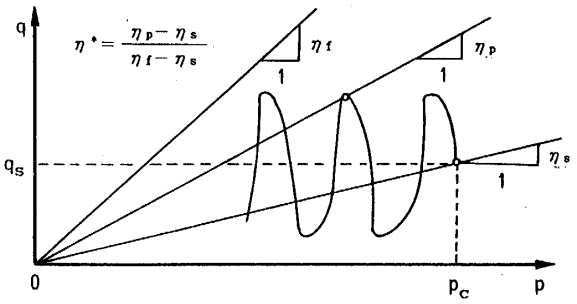

Fig.13 Schematic diagram for relative effective stress ratio $\eta^*=(\eta_p-\eta_s)/(\eta_f-\eta_s)$

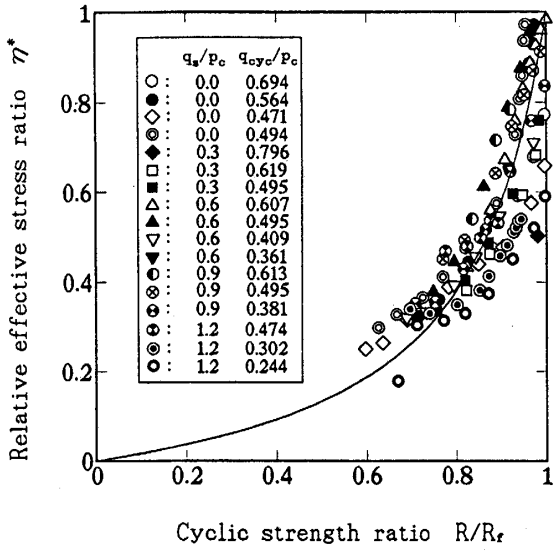

Fig.14 Relationship between relative effective stress ratio η^* and cyclic shear strength ratio R/R_f

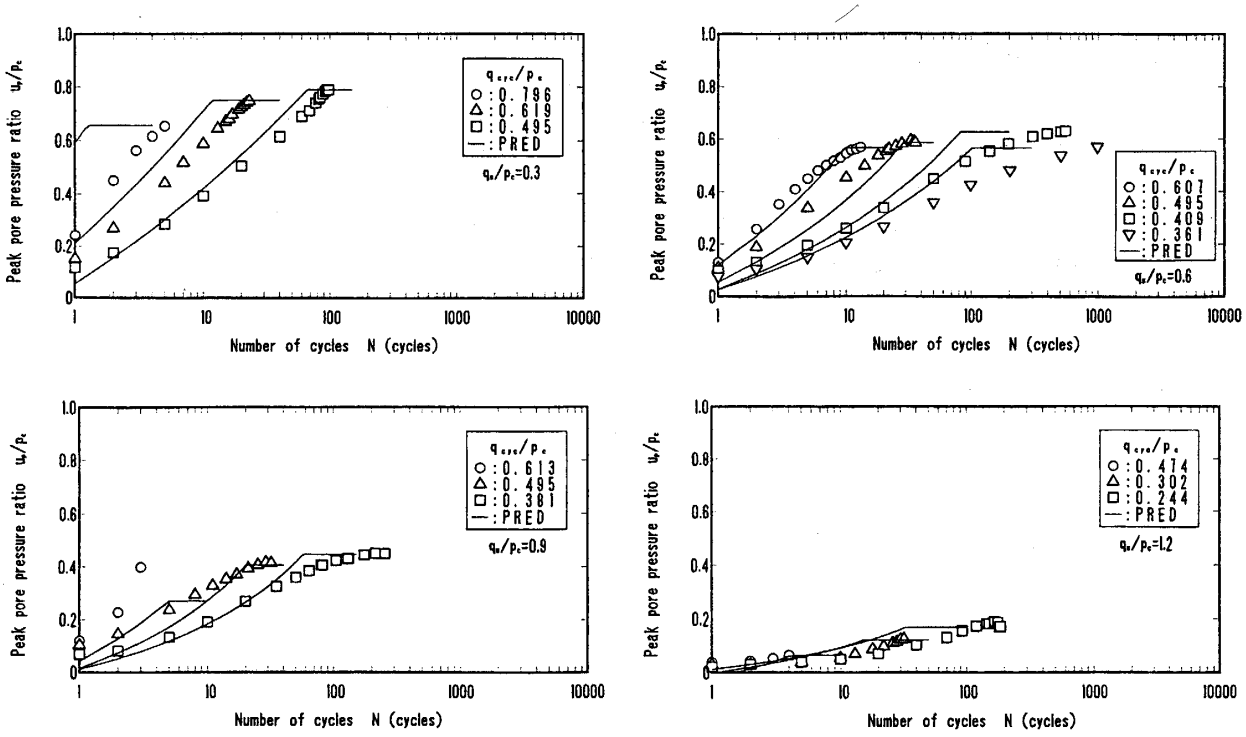

Fig.15 Predicted and experimental accumulated peak pore pressure

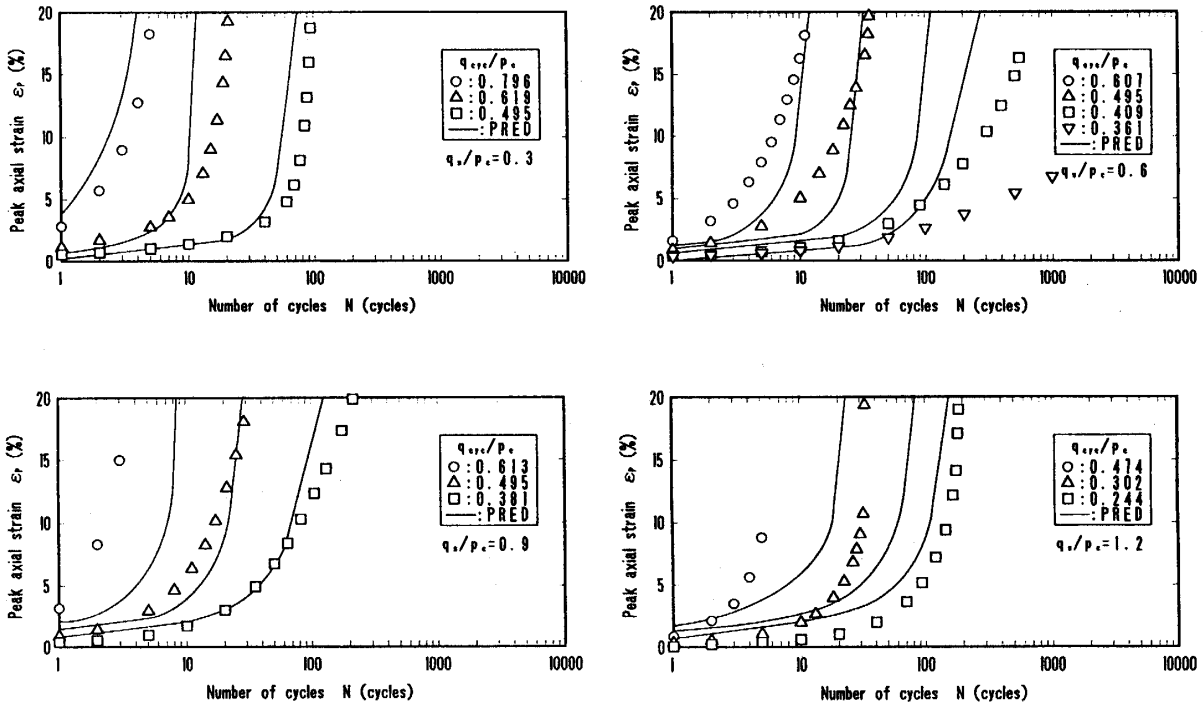

Fig.16 Predicted and experimental accumulated peak axial strain

cyclic loading. The predicted and observed pore pressures and axial strains are presented in Figs.15 and 16 in which the results for each initial static and subsequent cyclic shear stresses are illustrated. In these figures, the predicted and observed results correspond to solid lines and plots, respectively.

Fairly good correspondence is observed between predicted and experimental results in spite of very complicated initial conditions. Therefore, it is confirmed that the proposed model is a reasonable method for accumulating the cyclic-induced shear strain of clay subjected to various magnitudes of initial static and subsequent cyclic shear stresses.

Post Cyclic Recompression of Isotropically and Anisotropically Consolidated Clay

Samples which failed under undrained cyclic loading were allowed to reconsolidated when measurements of volumetric strain were taken after full dissipation of the residual pore water pressure. Fig.17 shows the relationship between the post cyclic volumetric strain and the normalized residual pore water pressure. There is a unique non-linear relationship which includes points for all initial isotropic and anisotropic consolidation conditions.

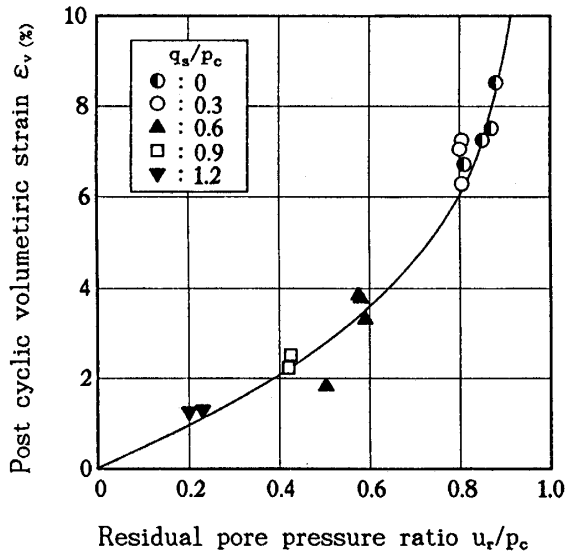

Fig.17 Relationship between post cyclic volumetric strain and normalized maximum residual pore pressure during undrained cyclic loading

Conclusions

In order to evaluate the cyclic shear strength and deformation of clay with the initial static shear stress, a series of cyclic triaxial tests was performed. A semi-empirical model for accumulating cyclic-induced axial strain is proposed. The model can evaluate the residual shear strain of clay at various magnitude of initial static shear stress.

References

1) Seed, H.B., Romo, M.P., Sun, J.I., Jaime, A. and Lysmer, J., "Relationships between soil conditions and earthquake ground motions in Mexico City in the Earthquake of September 19, 1985", Report No.UCB/EERC-87/15, Univ. of Carifornia, Berkeley, (1987).
2) Mendoza, M.J. and Auvinet, G., "The Mexico Earthquake of September 19, 1985 - Behaviour of Building Fcundations in Mexico City", Earthquake Spectra, 4, [4] , 835-852 (1988).
3) Sasaki et al., "Earthquake damage of soil structures", Report of Public Research Institute, No. 1576, (1980), (in Japanese).
4) Andersen, K.H., Kleven, A. and Heien, D., "Cyclic soil data for design of gravity structures", Proc. ASCE, 114, [GT5] , 517-539 (1988a).
5) Andersen, K.H. and Lauritzen, R., "Bearing capacity for foundations withc cyclic loads, Proc. ASCE, 114, [GT5] , 540-555 (1988b).
6) Yamamoto, Y., Hyodo, M., Murata, H., Yasufuku, N. and Sugiyama, M., "Effects of frequency on undrained cyclic shear characteristic of clay", The 27th Japan National Conference on Soil Mechanics and Foundation Engineering, 903-906, (1992).
7) Hyodo, M., Murata, H., Yasufuku, N. and Fujii, T., "Undrained cyclic shear strength and residual shear strain of saturated sand by cyclic triaxial tests", Soils and Foundations, 31, [3] , 60-76, (1991).
8) Hyodo, M., Yasuhara, K. and Hirao, K.: "Prediction of clay behaviour in undrained and partially drained cyclic triaxial tests", Soils and Foundations, 32, [4] , 117-127 (1992).
9) Hyodo, M., Sugiyama, M., Yamamoto, Y. and Kawata, Y., "Evaluation of pore pressure and strain of normally consolidated and overconsolidated clay subjected to cyclic shear stress", Proc. Japanese Society of Civil Engineers, (submitted), (in Japanese).
10) Hyde, A.F.L. and Ward, S.J., "A pore pressure and stability model for a silty clay under repeated loading", Geotechnique, 35, [2] , 113-125 (1985).